

Partial State-Feedback Reduced-Order Switching Predictive Models for Next-Generation Optical Lithography Systems

Raaja Ganapathy Subramanian^{a,b,1,*}, Barry Moest^{b,2}, Bart Paarhuis^{b,3}

^a*Eindhoven University of Technology, The Netherlands.*

^b*ASML NV, The Netherlands.*

Abstract

This paper presents a partial state-feedback reduced-order switching predictive model designed to support the next-generation lithography roadmap. The proposed approach addresses the trade-off between increasing the number of measurements to improve overlay accuracy and the resulting challenges, including higher measurement noise, reduced throughput and overlay/placement errors under uncertain operating conditions.. By minimizing (die-) placement errors and reducing unnecessary measurements, the method enhances system performance and throughput. Our solution employs a streamlined model with adaptive switching logic to manage time-varying uncertainties induced by fluctuating operating conditions. The methodology is implemented on a state-of-the-art lithographic scanner to mitigate the spatial-temporal dynamics of reticle heating, serving as a representative industrial application. Reticle heating, which worsens with increased throughput, introduces spatial-temporal distortions that directly degrade die placement accuracy. Experimental results demonstrate significant improvements: placement errors are reduced by a factor of 2 – 3x, and throughput is improved by 0.3seconds per wafer. Importantly, the method accounts for the fact that increased throughput can exacerbate reticle heating, which directly impacts overlay performance. By actively compensating for these thermomechanical effects, the proposed approach ensures that overlay accuracy is maintained or improved – even under increased throughput conditions – highlighting its potential for broader application in advanced lithographic systems, particularly in thermal and vibration control.

Keywords: Reticle heating, spatial-temporal systems, switching-models, lithography systems and scanners, model-reduction, partial state-feedback.

*Corresponding author

Email addresses:

raaja.ganapathysubramanian@asml.com,

r.g.subramanian@tue.nl (Raaja Ganapathy

Subramanian), barry.moest@asml.com (Barry Moest),

bart.paarhuis@asml.com (Bart Paarhuis)

¹Mobile number: +31 682613549

1. INTRODUCTION

We are living in an age dominated by information technology, which is widely considered to have truly begun with the creation of transistors followed by the development of an integrated circuit (IC). Since then, information technology has experienced rapid exponential growth. Similarly, electronics has transitioned from using circuits made of discrete components soldered to a printed circuit board to ICs comprising billions of interconnected transistors on a single chip. These chips provide alternatives to traditionally large and costly discrete optical devices and allow for new applications that traditional techniques could not achieve. This expansion has been driven by exponential advances in computing power, data storage, and communication. This remarkable growth is commonly referred to as Moore's law [1, 2], despite not being a physical law and serving more as an economic hypothesis. For more than 50 years, Moore's prediction has acted as a guiding principle for the semiconductor industry.

Photolithography is the most essential technique in the entire semiconductor production process for determining the scale at which chip elements can be created. It is responsible for transferring the layout of the circuit to the raw material, eventually transforming it into ICs using sophisticated

machines [3], as illustrated in Figure 1. In photolithography, the illuminator generates a (deep/extreme) ultraviolet light (DUV/EUV) beam, which is manipulated through an optical system to interact with a pattern on a quartz/zerodur plate, known as the reticle, thus forming an image on a thin layer of photosensitive material (resist) atop a circular silicon substrate, the wafer. Typically, the minimum feature size in this projection ranges from 3 [nm] to 500 [nm], achieving precision in the order of subnanometers, commonly termed overlay performance or placement errors [4]. Economically, high throughput is essential [5, 6, 7, 8], requiring high operating speeds that introduce disturbances that affect desired performance. To push the limits in the lithography industry, a shift toward model-based prediction and control has been implemented to achieve high-performance goals using raw data [9, 10, 11, 12]. However, these systems can experience various disturbances that cause non-linear behavior. The limitations of linear prediction and control, affected by the “water-bed effect [13, 14, 15, 16],” have prompted a movement towards nonlinear methods, including nonlinear variable gain control [16], filters [15, 11, 10], and switched controllers [13, 14]. Although these methods improve performance in the time domain, they often overlook spatial-temporal behavior [11] in lithography processes. Despite research in this field [17, 18], practical application of advanced

²Mobile number: +31 614611085

³Mobile number: +31 623016707

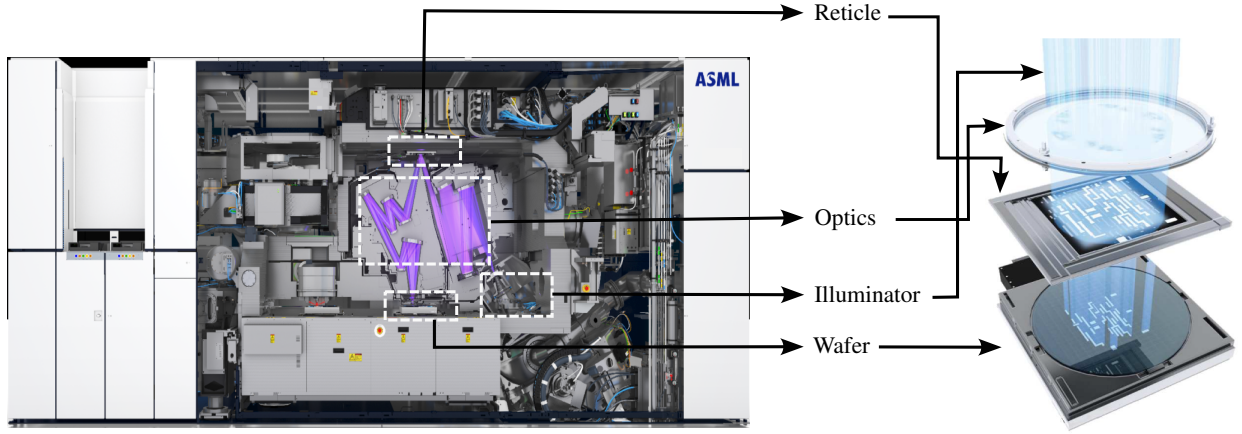


Figure 1: An illustration showing an ASML Twinscan and the exposure process with a lens, reticle, and wafer from top to bottom [3].

models and control is limited due to challenges such as system complexity and unpredictability as mentioned below.

1. The complexity of system in real-time differs from simulations due to mismatched assumptions (e.g., full vs. partial state feedback).
2. Performance is limited by uncertainties and disturbances.
3. Ensuring global closed-loop stability in real time.
4. Balancing underlying physics characterization with simplicity.
5. Modularity, extendability, and implementation cost.

The first three factors directly influence system performance, specifically concerning overlay and

placement errors, while the fourth and fifth factors serve as practical limitations that often restrict the feasibility of suggested methods.

In order to connect theoretical concepts with practical applications while maintaining throughput and overlay efficiency, we propose a partial state-feedback reduced-order switching predictive model approach. This approach effectively handles uncertainties to enhance system performance, all while being straightforward, globally stable, and intuitively understandable. In this context, the primary contributions of the paper are as follows.

- To address the 1st, 4th, and 5th issues, we suggest employing reduced-order linear-time-invariant models derived from nominal large-scale systems. This involves selectively decoupling only the necessary spatial-temporal dynamics to maintain computational effi-

ciency.

- For the 2nd, a switching logic is proposed to tackle uncertainties related to physical effects.
- The method proposed for the 3rd demonstrates global uniform ultimate bounded asymptotic stability (GUAS) through the application of the small-gain theorem for nonlinear systems.
- Lastly, to demonstrate effectiveness, the proposed approach is tested on a state-of-the-art lithography system, specifically focusing on reducing the spatial-temporal impacts of reticle heating.

The structure of this paper unfolds as follows. Section 2 presents the proposed methodology and examines the stability attributes introduced by the control scheme. Section 3 gives an overview of a spatial-temporal system from the lithography setup, including the uncertain dynamics during reticle heating. Furthermore, we demonstrate the effectiveness of the method through experimental results from a cutting-edge lithography system, which is discussed further in Section 4. Section 5 offers concluding remarks, and the paper concludes with a future perspective in Section 6.

2. DESIGN OF PARTIAL STATE- FEEDBACK REDUCED-ORDER SWITCHING MODELS

This section begins with a step-by-step design philosophy in Section 2.1 and covers the closed-loop dynamics stability analysis in Section 2.2.

2.1. STRUCTURE OF THE PROPOSED METHODOLOGY

To implement the proposed methodology in real time, four main steps are required:

Step 1 – Integrating the Scheduler Φ and Closing the Feedback Loop. Examine the closed-loop control configuration depicted in Fig. 2, where the plant \mathcal{P} functions in response to an external input u_e . This input is affected by a time-dependent uncertainty Δ through an uncertain input channel u_Δ . The setup includes a reduced-order predictive switching model $\hat{\mathcal{P}}$ that uses partial state-feedback based on measured events y and aims at the desired result z . The predictive model also incorporates the scheduler Φ , which employs the history describing current and previous events, represented as $\mathcal{S} \in \{y, u_e, u_\Delta\} \forall T \in \{0, \dots, t_n\}$, to alternate between the applicable models. Our focus is on history-based switching, which selects the appropriate models using available information from y, u_e, u_Δ , as opposed to variable-gain control based that only changes the gain solely based on the magnitude of the feedback signal [19, 20, 21, 16, 22]

or its product with the signal and its derivative [23, 24, 25].

Remark 2.1. In the lithographic application considered in this work, the measured events y correspond to alignment sensor data, which only partially cover the reticle area, while the desired result z represents the full-wafer overlay map, available only after exposure.

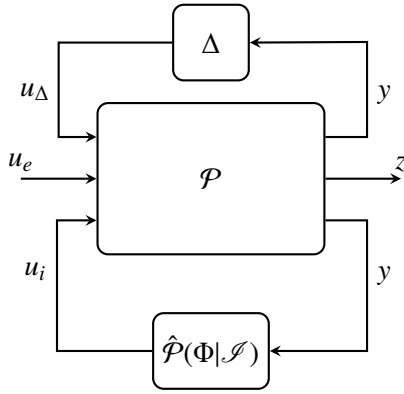


Figure 2: Simplified depiction of a partial state-feedback model with order reduction and switching in a closed-loop system.

The reasoning for the information \mathcal{I} -based switching Φ is outlined as follows:

- The feedback signal is partly unknown, as it originates from event-triggered feedback mechanisms;
- Feedback is accessible only during the production process, with no feedback available at other times;
- Modifying the proposed approach based on feedback signals or alternative methods would

necessitate a more intricate design;

- Historical information \mathcal{I} is consistently accessible, allowing us to optimize the use of the scheduler Φ to select suitable models.

In order to incorporate this in the proposed scheme, the scheduler Φ is chosen as follows:

$$\Phi = \{\mathcal{M}_i | \mathcal{I} \in \mathcal{R}_i \forall i \in \mathbb{Z}\} \quad (1)$$

Definition 2.1. An operating condition, referred to as a regime \mathcal{R} , is defined by the integration of a feedback signal y , an external signal u_e , and uncertainty u_Δ . The regime \mathcal{R}_i for $i = 0$ is identified as the nominal regime and is associated with a nominal model \mathcal{M}_0 . Conversely, for $i \neq 0$, it is described as the uncertain regime, which involves a set of uncertain models $\mathcal{M}_{i \in \mathbb{Z} \setminus \{0\}}$.

Consider an example using (1) with two distinct regimes: the nominal regime \mathcal{R}_0 and its associated model \mathcal{M}_0 , and another regime \mathcal{R}_1 , identified through \mathcal{I} . In this scenario, within regime \mathcal{R}_1 , we suppose $\{u_e, u_\Delta\} \in \emptyset$. Initially, with model \mathcal{M}_0 , the target performance z is achieved optimally when the system operates within regime \mathcal{R}_0 . However, if the system transitions to regime \mathcal{R}_1 due to the impact of y , the optimal performance of z is not maintained unless the scheduler Φ engages model \mathcal{M}_1 , appropriate for regime \mathcal{R}_1 . It is important to note that the choice of the nominal model greatly affects the performance of z . Thus, by effectively

configuring the scheduler Φ and selecting the nominal model \mathcal{M}_0 , we can merge the advantages and ensure optimal nominal and robust performance.

Remark 2.2. In (1), \mathcal{M} denotes the reduced-order model corresponding to different regimes \mathcal{R} of operating conditions. Upon the scheduler's detection of a regime shift, the model is updated, and the corresponding internal states are transferred from \mathcal{M}_k to \mathcal{M}_{k+1} .

Step 2 – Formulation of Nominal Reduced-Order Model. Partial differential equations govern spatial-temporal systems, as noted in [26, 18, 27], and are typically derived using finite-element models (FEM) or computational fluid dynamics (CFD) models. These large-scale models are often too complex for real-time application due to their high dimensionality (often exceeding $1e^6$) necessary for precise accuracy [11]. As an illustration, one method detailed in [28] runs a dynamic FEM alongside the physical system, providing real-time forecasts of the nominal spatial-temporal dynamics. This approach presents numerous modeling challenges, not only from theoretical and experimental standpoints, but also in ensuring robust performance.

To address this issue, model-order reduction techniques have been introduced, such as Balanced Truncation [29], Krylov's Subspace Methods [30], and the Proper Orthogonal Decomposition (POD) method [31]. These techniques are prevalent in var-

ious engineering domains. However, even though they decrease the dimensions of the FEM / CFD models, they often lose physical interpretability and continue to lack computational efficiency [18].

To achieve this, we apply a parametric reduction leveraging a Krylov's moment-matching method [32] that maintains the original physical interpretation of the reduced-order model. This approach can be expressed as ,

$$\mathcal{M}_i := \begin{cases} \dot{x}_i = A_i x_i + B_i u_e, \\ u_i = C_i x_i. \end{cases} \quad (2)$$

Remark 2.3. It is important to note that u_i in (2) is the estimated behavior of the underlying process, as shown in Fig. 2. The aim is to ensure that $\|z\| \rightarrow 0$

Step 3 – Using the partial feedback signal y to ensure that the model \mathcal{M}_i is up-to-date. In industrial settings, complete state feedback often demands considerable time and financial resources. Consequently, what is typically available is partial feedback, characterized by being limited and generally representing only a subset of the overall layout of physical effects. As a result, models deployed in such scenarios must accommodate these constraints. To integrate partial state-feedback into the reduced-order models discussed in the previous

section, we enhance (2) as follows: ,

$$\mathcal{M}_i := \begin{cases} \dot{x}_i = A_i x_i + B_i u_e + B_f u_f, \\ u_f = \Gamma(.)y, \\ u_i = C_i x_i. \end{cases} \quad (3)$$

This is achieved by explicitly incorporating an input channel B_f for feedback, with y representing the actual feedback measurements. In addition, in (3), a mapping function $\Gamma(.)$ is introduced. This function is designed to convert sparse feedback measurements into a suitable dense layout, using application-specific inputs. *It is important to note that the variable u_i in (2) and (3) is intentionally defined as such. The key lies in the definition of the information set \mathcal{I} , which is passed into the functional $\hat{\mathcal{P}}(\Phi|\mathcal{I})$. This set comprises the exogenous input u_e , the measured output y , and the uncertainty term u_Δ . To reformulate the problem in the 9-gang framework, the partial output measurement y is incorporated into the feedback loop, and the information set \mathcal{I} is treated as a variable within the functional representation of $\hat{\mathcal{P}}$.*

Step 4 – Transforming reduced-order models \mathcal{M}_i to incorporate uncertainty. To efficiently manage uncertainties as highlighted in Section 2.1, the framework is divided into a nominal model, denoted as \mathcal{M}_0 , alongside a collection of uncertain models, represented by \mathcal{M}_Δ . By employing a centering method [33], we express these models in the form:

$$\hat{\mathcal{P}}(\Phi|\mathcal{I}) = \mathcal{M}_n + \mathcal{M}_\Delta = \mathcal{M}_n + \Delta_m(\Phi|\mathcal{I}), \quad (4)$$

, where $m = \arg \max_m \Phi$.

Here, \mathcal{M}_n serves as the nominal model, while $\Delta_m(.)$ represents the set of uncertain dynamical models. It is apparent from the equation (4) that the collection of models belongs to the category of Lur'e-type systems [34], which integrate both a linear dynamical component and a nonlinear/uncertain one.

Remark 2.4. It is crucial to observe that the system depicted in Fig. 2, following the prior transformation, also falls under the Lur'e-type system category. This is a key point for analyzing closed-loop stability in future discussions.

Furthermore, this approach ensures that the uncertain dynamics is bounded, specifically $\|\Delta_m(.)\|_\infty \in \mathbb{R}$, and modulated by the scheduler Φ according to (1). *Finally, the scheduler mechanism can explicitly defined as follows:*

$$\Phi := \begin{cases} i \in \mathbb{Z} \\ \text{if } \mathcal{R}_i(\mathcal{I}_t) \geq \mathcal{R}_j(\mathcal{I}_t), \forall j \in \mathbb{Z}_{\setminus\{0\}}, t \in \mathbb{R}_{\geq 0} \\ \mathcal{I}(.) \in \{y, u_e, u_\Delta\} \end{cases} \quad (5)$$

Remark 2.5. The specific definition of the regime \mathcal{R} is application-dependent and will vary based on the context, objectives, and characteristics of the input signals $\mathcal{I}(.) \in \{y, u_e, u_\Delta\}$. As such, \mathcal{R} should

be designed to reflect the performance criteria or priorities relevant to the particular system under consideration.

2.2. STABILITY ANALYSIS

To conduct a stability analysis of the dynamic behavior influenced by the proposed approach, we utilize Fig. 2, (3), (4), along with the generalized-plant framework as defined in [33]. We transform the closed-loop system to a Lur'e-type system, illustrated in Fig. 3. The closed-loop dynamics can be minimally realized by integrating the uncertainty with the nominal predictive model, employing upper and lower linear-fractional-transformations (LFT) as outlined respectively in [33]:

$$\begin{bmatrix} \dot{x} \\ y \\ z \end{bmatrix} = \begin{bmatrix} \mathcal{A} & \mathcal{B}_e & \mathcal{B}_f & \mathcal{B}_i \\ C^y & \mathbb{O} & \mathcal{D}_f^y & \mathcal{D}_i^y \\ C^z & \mathbb{O} & \mathcal{D}_f^z & \mathcal{D}_i^z \end{bmatrix} \begin{bmatrix} x \\ u_e \\ u_f \\ u_i \end{bmatrix}, \quad (6a)$$

$$u_i = \Delta_m(\Phi|\mathcal{I}), \quad (6b)$$

with the uncertainty defined as:

$$\Delta := \begin{cases} \dot{x}_\Delta = A_\Delta x + B_\Delta u_f, \\ u_f = \Gamma(\cdot)y, \\ u_\Delta = C_\Delta x_\Delta + D_\Delta u_f. \end{cases} \quad (7)$$

Remark 2.6. To account for deviations between predicted and actual system behavior, we introduce an additive uncertainty model in Equation (6). This

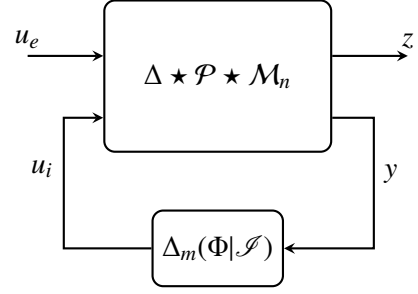


Figure 3: Schematics of the proposed methodology in a Lur'e-type system. Note that the \star denotes the LFT operator.

uncertainty captures the effects of unmodeled dynamics, and parameter variations. It is computed by first defining a nominal model based on the reduced-order dynamics and switching logic. The residuals between the model predictions and observed outputs are then analyzed over a validation dataset. The resulting uncertainty is characterized as a bounded additive error term, statistically quantified using confidence intervals. This formulation allows the control design to explicitly account for model inaccuracies and improve robustness.

Assumption 2.1. The closed-loop dynamics of the actual plant, when compensated using the nominal reduced-order partial state-feedback denoted as $\Delta \star \mathcal{P} \star \mathcal{M}_n$, fits within the category of globally uniformly ultimately bounded asymptotically stable systems.

Remark 2.7. It's important to observe that Assumption 2.1 is relatively mild. Indeed, lacking these conditions would impede the integration of predictive models into a stable closed-loop, thereby preventing the achievement of the system's nomi-

nal performance.

Remark 2.8. Let us consider x^\star to be the equilibrium point of (6) such that $\|z\| \rightarrow 0$. It is important to note that x^\star is the sole equilibrium point with the property that $\|z\| = 0$, because the minimum state-space representation in (6) ensures observability. This means that the observability matrix is of full rank, and hence, the system of equations $z = 0, \partial z / \partial t = 0, \dots, (\partial^{n-1} z) / (\partial t^{n-1}) = 0$ yields a unique solution x^\star , when $\|z\| \rightarrow 0$.

Using the small-gain theorem as specified in [13, 19, 35] together with the stability theorem presented in [16], the global uniform ultimate bounded asymptotic stability can be guaranteed. As a result, under such conditions, it is possible to precisely forecast the dynamics of the plant, which implies that $\|z\|$ will be reduced to zero for all $t \in \mathbb{R}$.

3. LITHOGRAPHY SYSTEM APPLICATION: RETICLE HEATING

In this section, we will implement the proposed methodology on a high-precision industrial optical system, specifically an ASML Twinscan, as shown in Fig. 1. These systems, utilized for the production of ICs, operate so that during standard production, light is absorbed by the reticle as it progresses toward the lens, as shown in Fig. 4. The reticle is usually positioned on a clamp. The chrome absorber layer, which delineates the pattern on the reticle, absorbs this light during exposure, caus-

ing it to heat up; this phenomenon is termed reticle heating (RH). Moreover, depending on the specific layer that is exposed, the reticle may feature a pellicle, serving as a protective barrier against contamination. In addition, heat dissipation occurs from both the upper and lower sides of the reticle to the surroundings, and there is a cooling flow designed to mitigate the effects of reticle heating. In typical manufacturing cycles, a wafer batch is exposed using a reticle, commonly referred to as a lot. Consequently, the reticle undergoes frequent thermal cycling, as depicted in Fig. 5. During this process, the temperature of the reticle rises upon exposure of each wafer (approximately tens of seconds), and it does not sufficiently cool during the wafer exchange period (less than a few seconds). This results in a significant temperature gradient between the first and last wafers in a lot. Overall, the global heating trend follows an exponential progression over time, leading to distortions in the image projected onto the wafer. Additionally, once a lot is fully processed, not only do the wafers need replacement with a new batch, but the reticles do as well. This replacement involves unclamping and reclamping the reticle from the reticle stage, introducing variability that alters the thermomechanical boundary conditions of reticle heating dynamics (RH). As shown in Fig. 5, RH physics also demonstrates spatial-temporal characteristics [36, 37, 38, 39]. The extent of these dom-

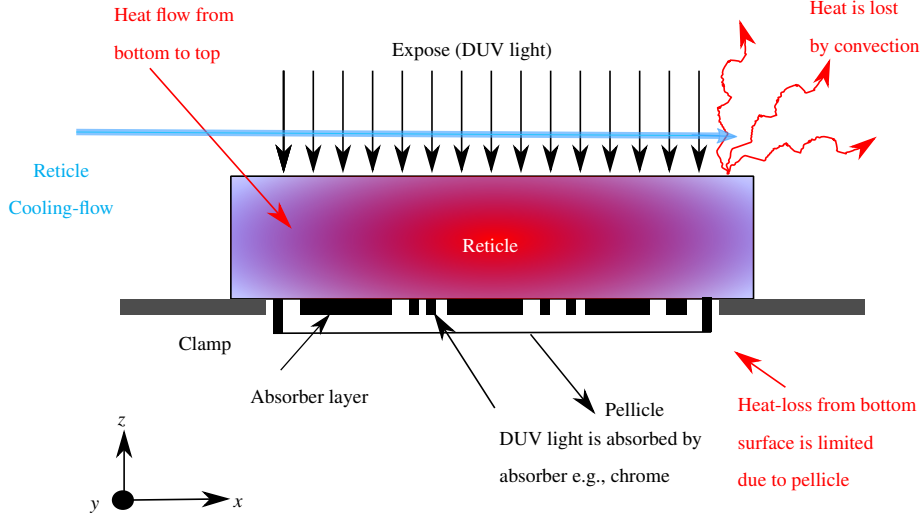


Figure 4: Artistic impression of reticle heating physics.

inant spatial-temporal distortions presents a significant challenge, particularly for high-throughput and high-performance systems. This aspect of the process is of primary interest in this manuscript.

Remark 3.1. We focus on placement/overlay errors in $x - y$ and ignore z for simplicity.

Before we proceed to discuss the experimental results in Sections 3.2, we shall assess the stability conditions established in Section 2.2, as detailed in Section 3.1.

3.1. STABILITY CONDITIONS

The reticle is constructed from physical materials and during its heating process, energy absorption results in deformations. Thus, reticle heating displaying unbounded dynamics is practically unlikely. Applying similar reasoning, we can draw analogous conclusions for the nominal model \mathcal{M}_n

and the specific models that represent the uncertain dynamics characterized by $\Delta_m(\Phi|\mathcal{J})$. Furthermore, utilizing the design methodology described in Section 2.1, we identify 3 moments that describe both the nominal and uncertain reticle heating models. Consequently, it is reliable to say that the dynamics of the actual system and the nominal model in a closed loop, namely, $\Delta \star \mathcal{P} \star \mathcal{M}_n$, comply with the assumption 2.1. In addition, we adopt the uncertain model definition given by (6). Therefore, as demonstrated in Section 2.2, all necessary conditions are met to ensure that the equilibrium point x^* (where $\|z\| = 0$), reached by applying the proposed method (6), is GUAS. ■

3.2. EXPERIMENTAL RESULTS

To evaluate and measure how the proposed method performs with respect to throughput and overlay placement errors, a series of real-time mea-

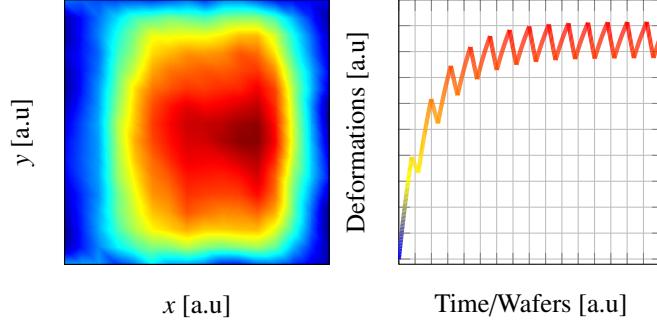


Figure 5: Spatial-temporal dynamics of the reticle heating.

measurements is obtained, as depicted in Fig. 6. In this experiment, initially, during the regime labeled as \mathcal{R}_a , the heating of the reticle shows standard behavior (without uncertainty) and gradually heats up to its saturation level. Subsequently, the reticle used in \mathcal{R}_a is released, transitioning to a new regime \mathcal{R}_b , where different dynamics and boundary conditions apply. Consequently, when the reticle returns for a second series of exposures and is re-clamped, it tends to display the dynamics characteristic of \mathcal{R}_c due to the altered boundary conditions resulting from the re-clamping process. Ini-

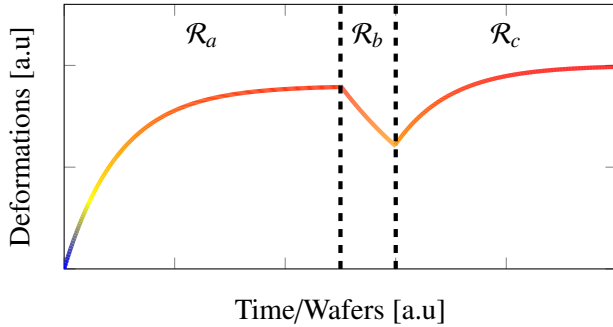


Figure 6: Experiment triggering nominal and uncertain conditions.

tially, we evaluated throughput performance relative to the current approach illustrated in Fig. 7, which utilizes top-bottom-edge alignment marks as detailed in [17], with measurements conducted for each wafer. Typically, additional alignments incur time costs as a result of the requirement for physical measurements. In this scenario, each measurement takes approximately 0.3s per wafer. By adopting the proposed methodology, we implement a spatial-temporal prediction model to characterize the RH across the entire reticle. Leveraging this model allows us to bypass the need for edge-alignment marks, substituting measurements with predictive estimates. Specifically, we used measurements from top-bottom alignment marks (see Fig. 7) combined with the models discussed in Section 2 to predict z and delineate the RH physics throughout the reticle. Consequently, this approach saves 0.3s per wafer, which can lead to an increase of up to 7 wafers per hour, a significant improvement for throughput. In Fig. 8, we present a

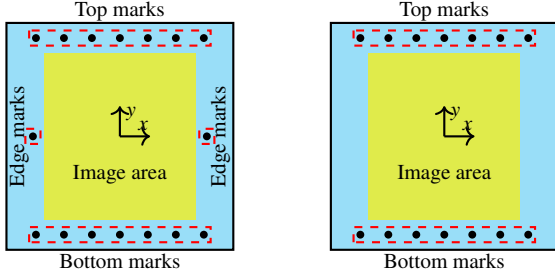


Figure 7: Exposure layout with varying alignment marks; reticle is exposed in the image area.

comparative analysis of the overlay placement error performance. This analysis is not only conducted against the current standard [17], but also against a linear version of our proposed approach that solely relies on the nominal model \mathcal{M}_n under all conditions. This latter comparison highlights the critical need for careful application of model-based predictions in industrial scenarios, as misuse can lead to significant performance drawbacks. Additionally, an experiment detailed in Fig. 6 was conducted over 2 lots, with each lot comprising of 16 wafers. It is observable that the placement error associated with the proposed methodology exhibits greater stability and improved accuracy in both the $x - y$ direction compared to the current method, under both nominal and uncertain conditions. Furthermore, the linear counterpart of the proposed technique experiences up to 3x reduction in performance due to unknown uncertainties. Notably, with the adoption of the proposed approach, the performance of the first 2 wafers in the $x - y$ direction shows a 2x improvement over the conven-

tional method. Additionally, the proposed methodology achieves performance that is either comparable or superior even without the need for measuring additional alignment marks. Consequently, while increasing throughput by up to 7 wafers per hour, the overlay placement errors remain stable and enhanced.

Remark 3.2. Under nominal conditions, both the proposed methodology and its linear counterpart perform identically, as their predictions remain unchanged \mathcal{R}_a .

Remark 3.3. Placement errors should not be negative; negative values are used for illustration only.

Remark 3.4. Equation (3) incorporates partial state feedback through the term $u_f = \Gamma(.)y$, where y represents real-time sensor measurements. Although y may appear comprehensive, it only captures localized observations from alignment sensors, thus providing partial information about the system state. The mapping function $\Gamma(.)$ translates these sparse measurements into the input space of the predictive model. In the context of reticle heating, Γ encodes the spatial relationship between alignment mark coordinates and the predicted heating locations, effectively bridging the gap between partial observations and the full-state input required for control. This design enables the model to leverage available feedback while accounting for the spatial sparsity of the measurements. Given this choice, it is good to note that

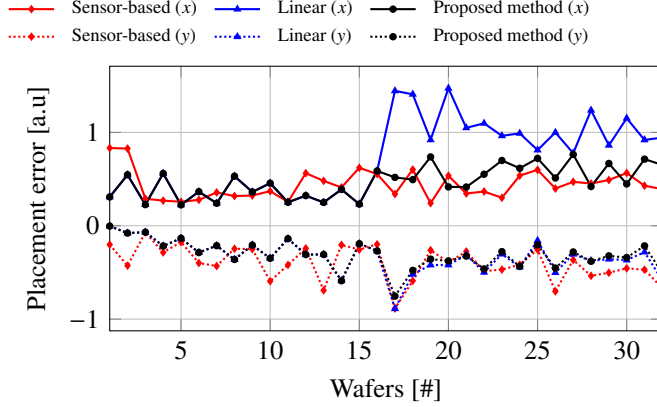


Figure 8: Placement error measurement in $x - y$ to compare the status-quo (red) against the proposed methodology (black) and its linear variant (blue).

the input channel B_f with respect to u_f reduces essentially to an identity matrix. This reflects a direct mapping between the feedback input u_f and the corresponding state components, which is appropriate given the structure of the reduced-order model and the nature of the partial feedback available in our application (with respect to reticle heating).

Remark 3.5. In the proposed switching predictive control framework, u_Δ is included as part of the switching input set. However, in the specific case of reticle heating, u_Δ represents a system-generated signal associated with events such as reticle reclamping. This signal is not directly measured; rather, its occurrence is inferred approximately based on system behavior. The timing of such events is only known retrospectively and with limited precision. Despite this, the framework is designed to handle such uncertainty by leveraging

historical patterns using other signals from \mathcal{I} and partial observations to infer the active regime, ensuring robustness even when certain inputs like u_Δ are not explicitly available in real time.

Remark 3.6. The effect of u_Δ on system behavior is output-dependent, as it alters the thermomechanical response of the reticle following a reclamp event. This dependency is discussed at the beginning of the experimental results section, where its influence on the output dynamics is illustrated.

4. DISCUSSIONS

In the context of customer interactions with our system during IC production, users may not exclusively utilize the image-area depicted in Fig. 7; they might opt for alternative image-areas as illustrated in Fig. 9. Our proposed approach is designed to be robust and remains applicable without the necessity for redesign or retuning despite these

on-the-fly layer changes. To demonstrate its efficacy, when conducting the same experiment with a reduced image-area, as illustrated in Fig. 9, Fig. 10 shows that the proposed methodology has improved the performance of both the nominal and uncertain regimes by a factor of 3x, while maintaining consistency. In contrast, similar to our previous findings, the linear version of the proposed method encounters significant challenges, leading to a performance decline of 2 – 3x compared to both the status quo and the proposed methodology. This demonstrates that the proposed approach al-

Importantly, there are no limitations on the order of the prediction models considered, and only output measurements are utilized. Furthermore, the GUAS of the equilibrium point is ensured and is naturally integrated into the design of the proposed methodology.

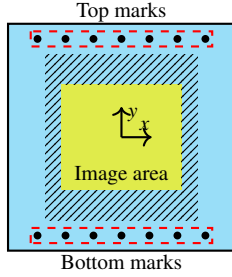


Figure 9: Schematic representation of small-exposure layout.

lows overlay placement errors to be comparable to or better than existing methods, while simultaneously enhancing system throughput. Additionally, it illustrates how state-of-the-art technologies can be integrated into industrial applications without sacrificing resilience, simplicity, and effectiveness. In conclusion, it is important to emphasize the intuitive nature of the proposed methodology. Linear and uncertain models can be employed via first-principle-based FEM with model reduction and data-driven system identification [40], respectively.

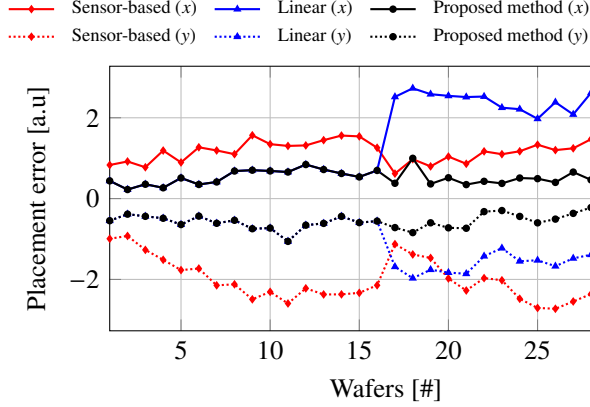


Figure 10: Placement error measurement in $x - y$ for a smaller image area (see, Fig. 9).

5. CONCLUSIONS

In this study, we introduce a partial state-feedback reduced-order switching predictive model designed to support the future lithography roadmap. This work addresses the balance between the demand for increased measurements, noise, and overlay errors (both within and across multiple wafers) under uncertain operating conditions. Our approach aims to navigate these trade-offs more effectively. This is accomplished by employing reduced-order linear models that can transition among various models based on a scheduling logic derived from historical data, thus handling time-varying uncertainties triggered by operating conditions. To address measurement configurations and maintain practical relevance, a partial state-feedback framework updates the model's internal states using these measurements. We establish sufficient criteria for global uniform ultimate bounded asymptotic stability through

time-regularization techniques. A generic execution method automates machine-in-the-loop initialization and execution of the methodology. The strategy is applied to a cutting-edge lithography scanner to mitigate the spatial-temporal dynamics of reticle heating. Experimentally significant improvements are achieved, with placement errors reduced by up to 2 – 3x and throughput enhanced by 0.3 [s] per wafer in all nominal and uncertain operating conditions. These results are compared to the current standard and the use of only the linear component of our proposed method.

6. FUTURE OUTLOOK

As previously mentioned in this manuscript, the relentless demand for high system productivity, coupled with the requirement to maintain equivalent or superior overlay accuracy and placement, influences and imposes demands on the enabling

methodologies. These models must, in essence, be resilient and capable of functioning in the midst of uncertainties. There are several key components to consider: 1) A unified predictive framework: although our main focus has been the reticle-heating subsystem, the entire assembly also experiences spatial and temporal variations across both lenses and wafers; 2) achieving enhanced throughput involves identifying and removing unnecessary measurements. Hence, a seamless integration of prediction, learning, and intelligence can allow measurement reductions without compromising overall system efficiency [41, 42, 43]; and lastly, 3) making plausible assumptions is crucial for practical deployment in industrial settings. The greater the disparity, the more challenging it becomes to reconcile theoretical concepts with practical applications. Consequently, the need is effectively summarized as the “development of approaches and techniques for designing adaptable and robust models for high-performance lithographic systems functioning in uncertain conditions while maintaining simplicity.” In conclusion, the authors anticipate that the findings reported herein will motivate further exploration and application of nonlinear and/or learning models in real-time systems to enhance performance and bridge the gap between theoretical insights and practical implementation.

REFERENCES

- [1] G. E. Moore, et al., Cramming more components onto integrated circuits (1965).
- [2] G. E. Moore, et al., Progress in digital integrated electronics, in: *Electron devices meeting*, Vol. 21, Washington, DC, 1975, pp. 11–13.
- [3] H. Butler, Position control in lithographic equipment: an enabler for current-day chip manufacturing, *IEEE control systems* 31 (5) (2011) 28–47.
- [4] V. Ishchuk, E. Guliyev, C. Aydogan, I. Buliev, M. Kaestner, T. Ivanov, A. Ahmad, A. Reum, S. Lenk, C. Lenk, et al., Scanning probe-based high-accuracy overlay alignment concept for lithography applications, *Applied Physics A* 123 (2017) 1–12.
- [5] T. Ito, S. Okazaki, Pushing the limits of lithography, *Nature* 406 (6799) (2000) 1027–1031.
- [6] C. Zahlten, P. Gräupner, J. van Schoot, P. Kürz, J. Stoeldraijer, W. Kaiser, High-na euv lithography: pushing the limits, in: *35th European Mask and Lithography Conference (EMLC 2019)*, Vol. 11177, SPIE, 2019, pp. 43–51.
- [7] B. Lüttgenau, S. Brose, S. Danylyuk, J. Stollenwerk, C. Holly, Investigation of the resolution limit of talbot lithography with compact euv exposure tools, in: *38th European Mask and Lithography Conference (EMLC 2023)*, Vol. 12802, SPIE, 2023, pp. 20–27.
- [8] I. Lee, J.-H. Franke, V. Philipsen, K. Ronse, S. De Gendt, E. Hendrickx, Hyper-na euv lithography: an imaging perspective, in: *Optical and EUV Nanolithography XXXVI*, Vol. 12494, SPIE, 2023, pp. 17–33.
- [9] R. G. Subramanian, M. Heertjes, T. de Hoog, A model-based inferential feedforward approach to deal with hysteresis in a motion system, in: *2018 Annual American Control Conference (ACC)*, IEEE, 2018, pp. 2934–2939.
- [10] F. Song, Y. Liu, D. Shen, L. Li, J. Tan, Learning control for motion coordination in wafer scanners: Toward gain

- adaptation, *IEEE Transactions on Industrial Electronics* 69 (12) (2022) 13428–13438.
- [11] M. F. Heertjes, H. Butler, N. Dirkx, S. van der Meulen, R. Ahlawat, K. O'Brien, J. Simonelli, K. Teng, Y. Zhao, Control of wafer scanners: Methods and developments, in: 2020 American Control Conference (ACC), IEEE, 2020, pp. 3686–3703.
- [12] F. Song, Y. Liu, J.-X. Xu, X. Yang, Q. Zhu, Data-driven iterative feedforward tuning for a wafer stage: A high-order approach based on instrumental variables, *IEEE Transactions on Industrial Electronics* 66 (4) (2018) 3106–3116.
- [13] B. Hunnekens, N. Wouw, D. Nešić, Overcoming a fundamental time-domain performance limitation by nonlinear control, *Automatica* 67 (2016) 277–281.
- [14] R. G. Subramanian, V. K. Elumalai, Discrete-time setpoint-triggered reset integrator design with guaranteed performance and stability, *ISA transactions* 81 (2018) 155–162.
- [15] C. Zheng, Y. Su, P. Mercorelli, A simple nonlinear pd control for faster and high-precision positioning of servomechanisms with actuator saturation, *Mechanical Systems and Signal Processing* 121 (2019) 215–226.
- [16] B. Hunnekens, N. van de Wouw, M. Heertjes, H. Nijmeijer, Synthesis of variable gain integral controllers for linear motion systems, *IEEE Transactions on Control Systems Technology* 23 (1) (2015) 139–149.
- [17] Y. H. Kim, J. Jang, B. S. Lee, H. Hwang, Y. Nam, J.-H. Kong, Y. S. Kang, S.-Y. Jang, B. Paarhuis, J. van der Wielen, et al., Reticle heating feed-forward control (rhc2) on nxt: 1980di immersion scanner for enhanced on-product overlay, in: *Optical Microlithography XXX*, Vol. 10147, SPIE, 2017, pp. 351–356.
- [18] C. Bikcora, S. Weiland, W. M. Coene, Thermal deformation prediction in reticles for extreme ultraviolet lithography based on a measurement-dependent low-order model, *IEEE Transactions on Semiconductor Manufacturing* 27 (1) (2014) 104–117.
- [19] B. S. Armstrong, J. A. Gutierrez, B. A. Wade, R. Joseph, Stability of phase-based gain modulation with designer-chosen switch functions, *The International Journal of Robotics Research* 25 (8) (2006) 781–796.
- [20] Y. Xu, J. M. Hollerbach, D. Ma, A nonlinear pd controller for force and contact transient control, *IEEE Control Systems Magazine* 15 (1) (1995) 15–21.
- [21] M. Heertjes, G. Leenknecht, Switching control in blu-ray disk drives, *Mechatronics* 20 (4) (2010) 453–463.
- [22] N. van de Wouw, H. Pastink, M. F. Heertjes, A. V. Pavlov, H. Nijmeijer, Performance of convergence-based variable-gain control of optical storage drives, *Automatica* 44 (1) (2008) 15–27.
- [23] S. Van den Eijnden, M. F. Heertjes, W. Heemels, H. Nijmeijer, Hybrid integrator-gain systems: A remedy for overshoot limitations in linear control?, *IEEE Control Systems Letters* 4 (4) (2020) 1042–1047.
- [24] B. Hunnekens, N. Wouw, D. Nešić, Overcoming a fundamental time-domain performance limitation by nonlinear control, *Automatica* 67 (2016) 277–281.
- [25] G. Zhao, D. Nešić, Y. Tan, C. Hua, Overcoming overshoot performance limitations of linear systems with reset control, *Automatica* 101 (2019) 27–35.
- [26] S. Afshar, F. Germ, K. Morris, Extended kalman filter based observer design for semilinear infinite-dimensional systems, *IEEE Transactions on Automatic Control* (2023).
- [27] R. F. Curtain, H. Zwart, An introduction to infinite-dimensional linear systems theory, Vol. 21, Springer Science & Business Media, 2012.
- [28] K. Nick, M. J. H. Lutikhof, Method of reducing effects of reticle heating and/or cooling in a lithographic process (Oct. 1 2019).
- [29] K. Willcox, J. Peraire, Balanced model reduction via the proper orthogonal decomposition, *AIAA journal* 40 (11) (2002) 2323–2330.
- [30] E. J. Grimme, Krylov projection methods for model reduction, University of Illinois at Urbana-Champaign,

- 1997.
- [31] L. Sirovich, Turbulence and the dynamics of coherent structures, parts i, ii and iii, *Quart. Appl. Math.* (1987) 561–590.
 - [32] D. Lou, S. Weiland, Parametric model order reduction for large-scale and complex thermal systems, in: 2018 European Control Conference (ECC), IEEE, 2018, pp. 2593–2598.
 - [33] S. Skogestad, I. Postlethwaite, *Multivariable feedback control: analysis and design*, John Wiley & sons, 2005.
 - [34] S. Mane, M. Mejari, F. Kazi, N. Singh, Improving life-time of fuel cell in hybrid energy management system by lure–lyapunov-based control formulation, *IEEE Transactions on Industrial Electronics* 64 (8) (2017) 6671–6679.
 - [35] P. Kokotović, H. K. Khalil, J. O’reilly, *Singular perturbation methods in control: analysis and design*, SIAM, 1999.
 - [36] C. Scherer, S. Weiland, *Linear matrix inequalities in control*, Lecture Notes, Dutch Institute for Systems and Control, Delft, The Netherlands 3 (2) (2000).
 - [37] P. Astrid, S. Weiland, K. Willcox, T. Backx, Missing point estimation in models described by proper orthogonal decomposition, *IEEE Transactions on Automatic Control* 53 (10) (2008) 2237–2251.
 - [38] K. Classens, T. Hafkamp, S. Westbeek, J. J. Remmers, S. Weiland, Multiphysical modeling and optimal control of material properties for photopolymerization processes, *Additive Manufacturing* 38 (2021) 101520.
 - [39] D. van den Hurk, S. Weiland, K. van Berkel, Performance-based active wafer clamp design for wafer heating effects in euv lithography, *IEEE Transactions on Semiconductor Manufacturing* 33 (3) (2020) 424–432.
 - [40] C. Yu, M. Verhaegen, Subspace identification of individual systems operating in a network (si²on), *IEEE Transactions on Automatic Control* 63 (4) (2018) 1120–1125.
 - [41] K. Friston, What is optimal about motor control?, *Neuron* 72 (3) (2011) 488–498.
 - [42] L. Kopitar, P. Kocbek, L. Cilar, A. Sheikh, G. Stiglic, Early detection of type 2 diabetes mellitus using machine learning-based prediction models, *Scientific reports* 10 (1) (2020) 11981.
 - [43] S. Oprea, P. Martinez-Gonzalez, A. Garcia-Garcia, J. A. Castro-Vargas, S. Orts-Escolano, J. Garcia-Rodriguez, A. Argyros, A review on deep learning techniques for video prediction, *IEEE Transactions on Pattern Analysis and Machine Intelligence* 44 (6) (2022) 2806–2826.